J. Electrochem. Sci. Eng. **13(6)** (2023) 1051-1061; http://dx.doi.org/10.5599/jese.1977

Open Access : : ISSN 1847-9286
https://pub.iapchem.org/ojs/index.php/JESE

Original scientific paper

Electrochemical evaluations of reduced graphene oxide for efficient counter electrode in dye-sensitized solar cell

Deependra Jhankal[1], Mohamad Saquib Khan[2], Krishna K. Jhankal[3] and Kanupriya Sachdev[1,2,✉]

[1]*Department of Physics, Malaviya National Institute of Technology, Jaipur 302017, India*
[2]*Materials Research Centre, Malaviya National Institute of Technology, Jaipur 302017, India*
[3]*Department of Chemistry, University of Rajasthan, Jaipur 302004, India*

Corresponding authors: ✉*ksachdev.phy@mnit.ac.in*; Tel.: 0141-2713382

Received: July 13, 2023; Accepted: September 22, 2023; Published: September 29, 2023

Abstract

The design and development of an alternative counter electrode (CE) using graphene-based low-cost material for the dye-sensitized solar cell (DSSC) is the major motivation of the current research to replace the traditional platinum counter electrode. Herein, we prepared reduced graphene oxide (rGO) and investigated it for an efficient CE in DSSC. The structural and morphological properties of rGO are analyzed using FESEM, TEM and Raman techniques. The performance of I_3^- reduction on the CE is characterized by the EIS Nyquist plot, cyclic voltammetry, and the Tafel curve. The measured electrochemical results suggested that rGO CE has a lower charge transfer resistance (R_{ct}), higher cathodic current density (J_{rd}), and higher Tafel slope as compared to graphene oxide (GO) CE, revealing that rGO CE has good catalytic activity towards the I_3^- reduction.

Keywords

Carbon nanomaterials; redox electrolyte; defect density; environmentally friendly synthesis; electrochemical performance

Introduction

Dye-sensitized solar cells (DSSCs) attained great potential because of ease of device construction, low manufacturing price, and good photo conversion efficiency [1]. Usually, DSSC contains a dye-absorbed anode, a redox electrolyte (*e.g.,* iodide/triiodide (I_3 / I_3^-) and a good-performing counter electrode (CE) [2] The CE holds the capability in order to boost DSSC conversion effectiveness by reducing triiodide into iodide ($I_3^- + 2e^- \rightarrow 3I^-$) [3]. Usually, in DSSC, the platinum (Pt) based FTO acts as CE due to its high conductivity [4]. Conversely, the high cost, poor stability, and insufficiency of Pt limit its use for the further development of CE in DSSC, which raises a need for alternative materials for CE.

Graphene is considered one of the most suitable materials for CE in DSSCs because it exhibits a large surface area due to its 2D structure, high mobility (10,000 cm^2 V^{-1} s^{-1}), good catalytic activity, and chemical stability [5-7]. The graphene-related advanced materials like graphene oxide (GO) and reduced graphene oxide (rGO) are also promising candidates for various applications due to their unique properties [8-10]. The oxidized form of graphene, known as GO, has carbon, hydrogen, and oxygen in variable ratios. The oxygenated functional groups present in GO are beneficial for their mechanical, electronic, and electrochemical properties. These functional groups reduce its electrical conductivity, which restricts the direct use of GO in electrocatalytic applications [11-13].

Reduced graphene oxide (rGO) is chemically derived graphene with astonishing features, including high mobility and good mechanical strength [14]. The oxygen groups present on GO sheets can be eliminated through the reduction process that produces rGO. Chemical methods are primarily used for the reduction of rGO using reducing agents that include sodium borohydride ($NaBH_4$), hydrazine (N_2H_4) and gallic acid [15-17]. These reducing agents make rGO hydrophobic by removing different oxygen functionality groups. In the reduction, the sp^2 carbon plane of GO is destroyed at many places and leaves sp^3 carbon vacancies that create holes and defects on the surface of graphene sheets [18]. These defects can provide a large number of active sites for catalytic activity. Although these reducing agents possess a superior ability to form high electrochemical-performing rGO for several applications, their toxicity and serious environmental impact hinder their further use for large-scale synthesis of rGO. To address these challenges, researchers all around the world have been working on *so-called* green reducing agents such as L-ascorbic acid, green tea extract, *opuntia ficus indica* and other plant extracts for the preparation of rGO. By using KOH and NaOH as reducing agents, the reduction rate of GO can be enhanced and some -OH functional groups added to the edges of graphene sheets. They restrict the restacking of the graphene sheets and enhance the contact area of the electrode and electrolyte, resulting in significant electrocatalytic performance [19-23]. Additionally, KOH and NaOH reducing agents considerably diminish the hazard and risk during the handling and washing of the final product and do not have any harmful impact on the environment compared to other toxic reducing agents.

Herein, we present a cost-effective and environmentally friendly method to synthesize rGO by using a mixture of NaOH and KOH as “green” reducing agent. Furthermore, the various physical parameters, including crystallite size and defect density, were obtained from Raman spectra results, which gives a comparative analysis of materials towards the catalytic activity. Different electrochemical techniques such as EIS, CV and Tafel curve were performed to investigate various electrochemical parameters such as diffusion coefficient (D), charge transfer resistance (R_{ct}), cathodic current density (J_{rd}) and Tafel slope to evaluate the in-depth kinetics study of rGO as an efficient CE for DSSC application.

Experimental

Materials

Potassium iodide (KI), graphite fine powder 325 mesh (99.8 %), hydrogen peroxide (H_2O_2 30 %), hydrochloric acid (35 %), titanium (IV) oxide nanopowder (99 %), sulphuric acid (95 to 97 %), carboxymethyl cellulose (CMC), and potassium hydroxide (KOH) were purchased from Alfa Aesar. Isopropanol alcohol (IPA), potassium permanganate ($KMnO_4$-99 %), iodine (I_2), acetonitrile, sodium hydroxide (NaOH), and ethylene glycol were procured from Fisher Scientific.

Preparation of electrode material (GO and rGO)

GO was prepared through the modified Hummer’s technique described in our previous work [16,24]. Initially, graphite in powder form was mixed in 50 ml of H_2SO_4 while stirring for 4 hours

in a conical flask. Then, $KMnO_4$ was slowly dissolved into the mixture while placing the flask in an ice bath. After that, 250 ml of de-ionized (DI) water was poured slowly under continuous stirring. H_2O_2 was added to the solution, resulting in a yellowish-brown color of the solution. The HCl solution was used to wash the obtained GO suspension (to eliminate metallic impurities). After that, the suspension was washed 3 to 4 times with DI water (pH ~7) using centrifugation and dried at 50 °C. Thereafter, rGO was obtained from the hydrothermal route (Scheme 1). 1 g GO flakes were added in a 60 ml solution of KOH and NaOH with a molarity ratio of 1:3. The solution was continuously stirred and sonicated for 1 hour, then shifted to a Teflon lined autoclave (100 mL) and heat treated at 160 °C for 12 hours in a hot-air oven. After the reaction was finished, the autoclave was left to cool naturally. The precipitate was collected and washed repeatedly with DI water. Finally, the washed black color residue was dried at 50 °C in the oven.

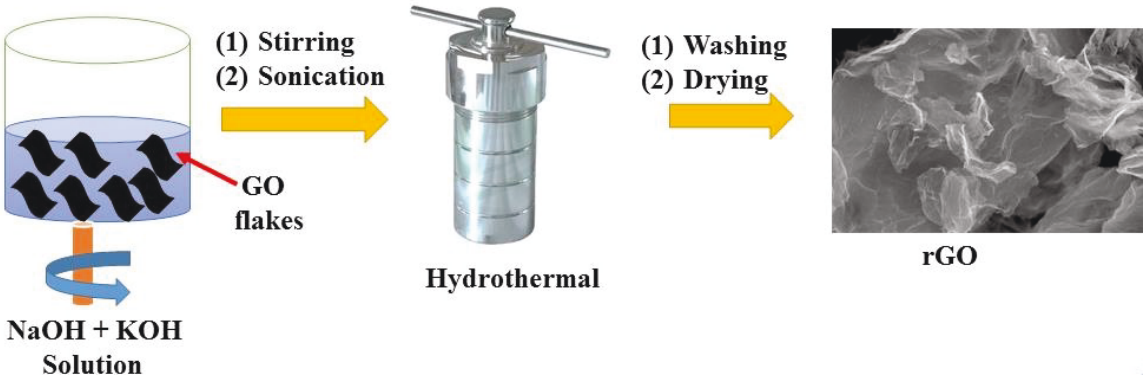

Scheme 1. *Pictorial presentation of synthesis process of rGO*

Preparation of electrolyte

For the preparation of (I^-/I_3^-) electrolyte, KI (2.16 g) and I_2 (0.42 g) were dissolved in a solution of acetonitrile (40 ml) and ethylene glycol (10 ml) and stirred for 60 minutes to get a homogenous mixture [25].

Preparation of CEs and fabrication of symmetric cells

The homogenous rGO paste was obtained through a simple grinding technique. Briefly, the 90 mg synthesized rGO powder and 10 mg of CMC (10 wt.%) were mixed in 10 ml of isopropanol alcohol and continuously ground in a mortar pestle. The prepared rGO slurry was drop casted onto ITO substrate (1×1 cm) and dried for 3 hours on the hot plate at 90 °C to fabricate rGO-CE. For GO-CE preparation, the same process was used.
Two types of symmetric cell GO/electrolyte/GO and rGO/electrolyte/rGO were fabricated using cellulose filter paper as a spacer. A few drops of a redox liquid electrolyte (I^-/I_3^-) solution were directly injected into the symmetric cells.

Characterization techniques

The surface microstructure of synthesized samples was analyzed by field emission scanning electron microscope (FESEM) and high-resolution transmission electron microscope (HR-TEM) using Nova Nano FESEM-450 and Tecnai G2 20 S-TWIN instrument. Samples were also examined by Raman spectroscopy by using a STR 500 confocal microspectrometer (wavelength = 532 nm). Electrochemical characterizations were recorded through the CHI instrument (CHI760E).

Results and discussion

Physicochemical analysis

The morphological study of the synthesized samples was conducted by the FE-SEM technique. The FESEM pictures of GO (Figure 1(a)) and rGO (Figure 1(b) and (c)) represent that the prepared samples have a sheet-type morphology. The highly exfoliated sheets in rGO are clearly shown in the FESEM image. The high exfoliation of rGO sheets could provide a large surface, which enhances the catalytic activity of CE [16].

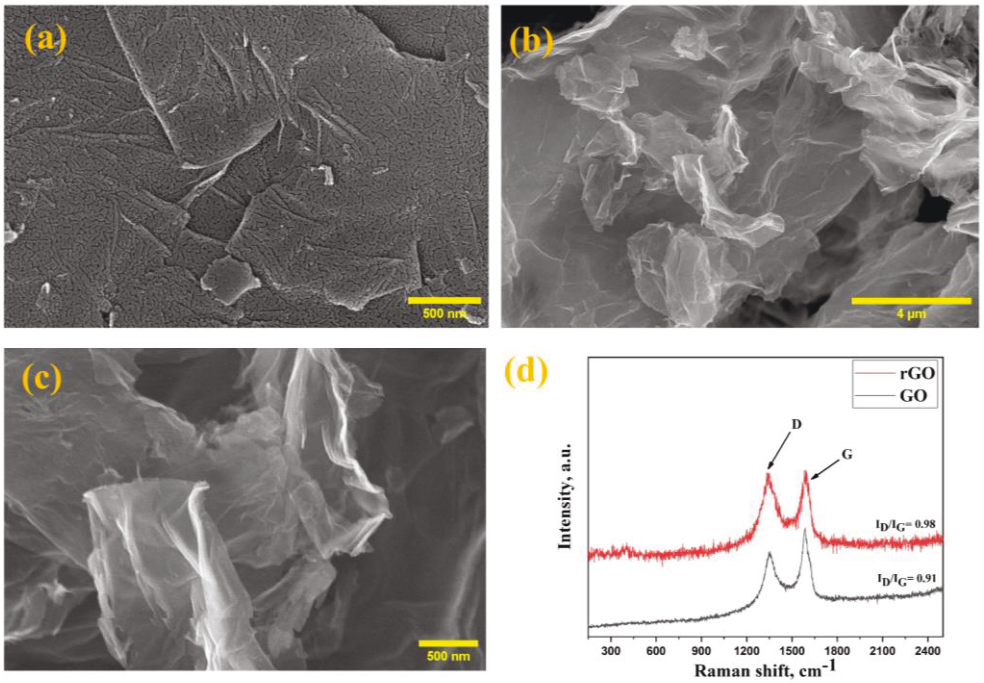

Figure 1. *FESEM images of prepared samples (a) GO and (b-c) rGO; (d) Raman spectra of GO and rGO*

Figure 1(d) represents the Raman curve of synthesized GO and rGO samples at 532 nm laser. In the Raman spectrum of rGO, the D band (~1354 cm^{-1}) and the G band (~1604 cm^{-1}) correspond to the defects present in the graphene sample and the vibration of sp^2 hybridized C- C atoms, respectively [26]. The intensity ratio of D to G band (I_D/I_G) value of rGO (0.98) is higher in comparison to GO (0.91). The high value of I_D/I_G for rGO makes it more suitable for electrocatalytic applications because high defects provide more sites for I_3^- reduction [27,28]. Using the equations (1) to (3), the value of I_D/I_G is used to calculate a number of physical properties of synthesized samples, including crystallite size (L_{Sp2} / nm), the mean distance of defects (L_D / nm), and density of defects (n_D, cm^{-2}) [29,30]:

$$L_{Sp^2} = \frac{560 I_G}{E_L^{\,4} I_D} \quad (1)$$

$$L_D^{\,2} = 2.4\times10^{-9} \lambda_L^{\,4} \frac{I_G}{I_D} \quad (2)$$

$$n_D = \frac{2.4\times10^{22} I_D}{\lambda_L^{\,4} I_G} \quad (3)$$

Here, E_L / eV implies energy and λ_L /nm refers to the wavelength of the laser source.

Table 1 lists the values of measured various physical parameters, including I_D/I_G ratio, which represent that rGO has a low crystallite size compared to GO. Additionally, the acquired value n_D is higher for rGO, indicating the existence of more defects overall in the sample, which further improves the catalytic activity of rGO-CE [29].

***Table 1**. Various physical parameters calculated from Raman analysis*

Sample	I_D / I_G	L_{sp2} / nm	L_D / nm	n_D / 10^{-11} cm^{-2}
GO	0.91	21.52	14.78	2.58
rGO	0.98	19.74	14.15	2.86

The TEM images of rGO at a high resolution of 200 nm and 50 nm are depicted in Figure 2(a) and Figure 2(b), respectively, indicating the transparent few-layer sheets of graphene. The exfoliated sheets structure of rGO could facilitate the large contact area with electrolyte and provide numerous active sites for reduction of I_3^- resulting in better performance of CE. The HR-TEM result (Figure 2(c)) shows the ordered structure of rGO with an interplanar distance of 0.41 nm. Selected area diffraction (SAD) pattern (Figure 2(d)) demonstrates the symmetrical hexagonal structure of graphene [31].

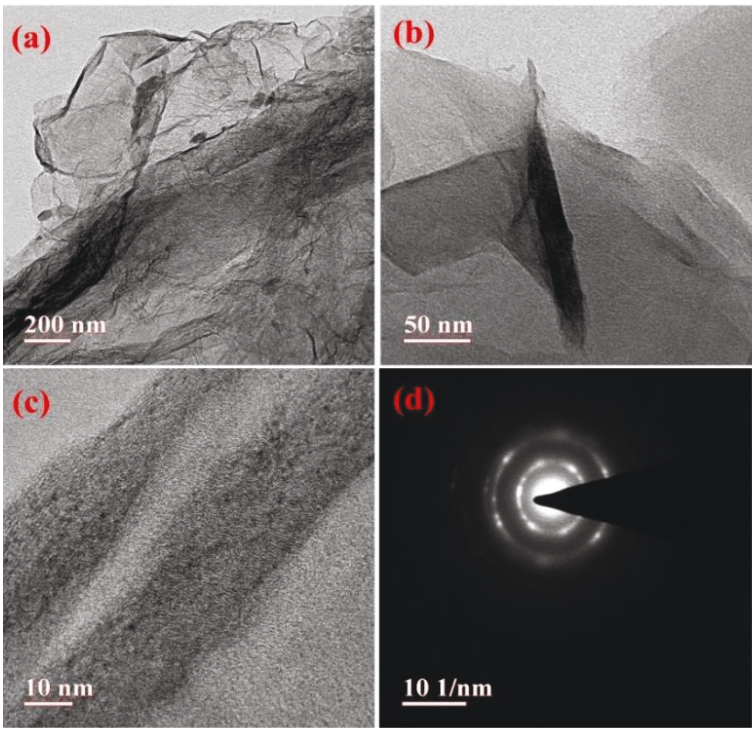

***Figure 2.** (a - b) TEM images, (c) HR-TEM image and (d) SAED configuration of rGO*

Cyclic voltammetry (CV) analysis of CEs

Cyclic voltammetry (CV) is mainly employed to evaluate the catalytic performance of CEs towards the reduction of I_3^- to $3I^-$ in DSSC. The catalytic profile of GO and rGO CEs, determined through CV analysis, are depicted in Figure 3(a). The oxidation and reduction peaks in the cyclic voltammogram represent the oxidation $3I^- - 2e^- \rightarrow I_3^-$ and reduction $I_3^- + 2e^- \rightarrow 3I^-$, respectively, which is significant for the CE performance in DSSC [32]. Cathodic peak current density (J_{red}) directly influences the performance of the CEs. For better electrocatalytic activity of CE, it should exhibit higher peak current density [33]. The rGO CE shows higher cathodic peak current density (J_{red1}) compared to GO CE because of the higher surface area and appropriate conductivity of rGO. Figure 3(b) shows cyclic voltammograms of rGO CE at several sweep rates (0.05 TO 0.3 V s^{-1}). Both peaks are shifted gradually

to the negative and positive sides, respectively. The anodic and cathodic peak current densities show good linear behavior with the square root of scan rate ($\nu^{1/2}$) (Figure 3(c)), which implies that only reduction of I_3^- occurred on the rGO-CE, and there is no particular interaction or reaction between redox-electrolyte (I^-/I_3^-) and rGO-CE during the electrochemical process [34].

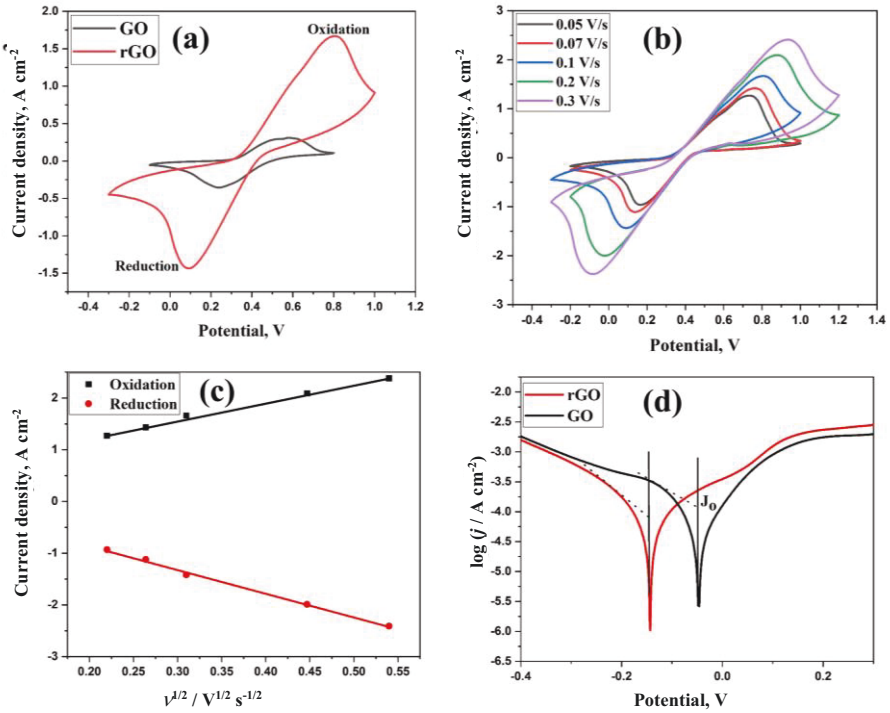

Figure 3. *(a) CV profiles of GO and rGO CEs at a sweep rate of 0.1 V s^{-1}; (b) CVs of the rGO CE at several sweep rates; (c) fitted linear curves of current density vs. $\nu^{1/2}$ dependence; (d) Tafel polarization curves*

The diffusion coefficient (D / cm^2 s^{-1}) of ions for both GO and rGO counter electrodes were obtained by Randles Ševčik equation [35] that is given by equations (4a) and (4b):

$$i_p = 0.4961nFAC\left(\frac{nFvD}{RT}\right)^{1/2} \quad (4a)$$

$$\frac{i_p}{\nu^{1/2}} = KACn^{3/2}D^{1/2} \quad (4b)$$

Here, i_p / A represents peak current, n refers to the number of electrons participating in redox reaction (n = 2), ν / V s^{-1} is the scan rate, C / mol cm^{-3}is concentration, A / cm^2 represents electrode area, and K is 298,633 (which accounts for the constant), F is Faraday constant, R is the ideal gas constant and T / K is the absolute temperature. The value of i_p / $\nu^{1/2}$ can be evaluated from the slope of the curve (Figure 3(c)). The obtained diffusion coefficient (D) of ions for the rGO counter electrode (4.74×10^{-11} cm^2 s^{-1}) is higher than that for GO CE (2.54×10^{-11} cm^2 s^{-1}). Higher diffusion coefficient for rGO-CE implies faster diffusion of ions through the electrode, which shows the superiority of the electrode material.

Impedance analysis of symmetric cells

The electrocatalytic profile of CEs was further investigated by electrochemical impedance spectroscopy (EIS) in the frequency range of 1 MHz to 1 mHz. The Nyquist plot of a symmetric cell includes two regimes. The diameter of the left semicircle at the high-frequency region shows the charge-transfer resistance (R_{ct}) at the CE and redox electrolyte interface. In comparison, the low-

frequency straight line regime represents the redox Nernst diffusion impedance (Z_N), which indicates the semi-infinite linear diffusion of redox couple in electrolyte [36]. The equivalent circuit of Nyquist plots comprises four components the: contact resistance (R_s), Nernst diffusion impedance (Z_N), double layer capacitance (C) and CE/electrolyte interface charge transfer resistance (R_{ct}). Among all these parameters, R_{ct} is the most significant for optimizing the electrocatalytic performance of the CEs in DSSC. The Nyquist plots of GO and rGO symmetric cells are shown in Figure 4(a) and their equivalent circuits are shown in the inset of Fig. 4(b). The EIS profiles of symmetric cells show that rGO has lower R_{ct} (25 Ω) than GO (600 Ω), which illustrates the significant catalytic ability of rGO towards the reduction of triiodide due to more defects present in rGO, which provides more catalytic sites for triiodide reduction. The R_s value of rGO (10.2 Ω) is lower than GO (18 Ω), which means that the contact resistance between rGO and ITO is reduced due to the better conductivity of rGO. Figure 4(b) shows the fitted EIS plot of rGO with the electrical equivalent circuit drawn in the inset. The Bode phase plot of rGO based symmetric cell is shown in the inset of Figure 4(b). The electrons are injected and recovered during the electrochemical catalytic activity and the diffusion length of transported electrons is equal to the square root of their diffusion coefficient and lifetime of electron ($L_n = (D_r \tau_r)^{-1/2}$). The characteristic frequency ($\omega_r = 1/\tau_r$) implies the finite diffusion of ions/electrons in CE where interfacial redox reactions in the CE are hindered [37]. The electron lifetime (τ_r) can be determined by equation (5):

$$\tau_r = \frac{1}{2\pi f_{max}} \tag{5}$$

where f_{max} / Hz is the frequency of the maximum in the Bode phase plot. The obtained τ_r of rGO based symmetric cell is 73 µs, representing a fast movement of electrolyte ions during the catalytic activities [38].

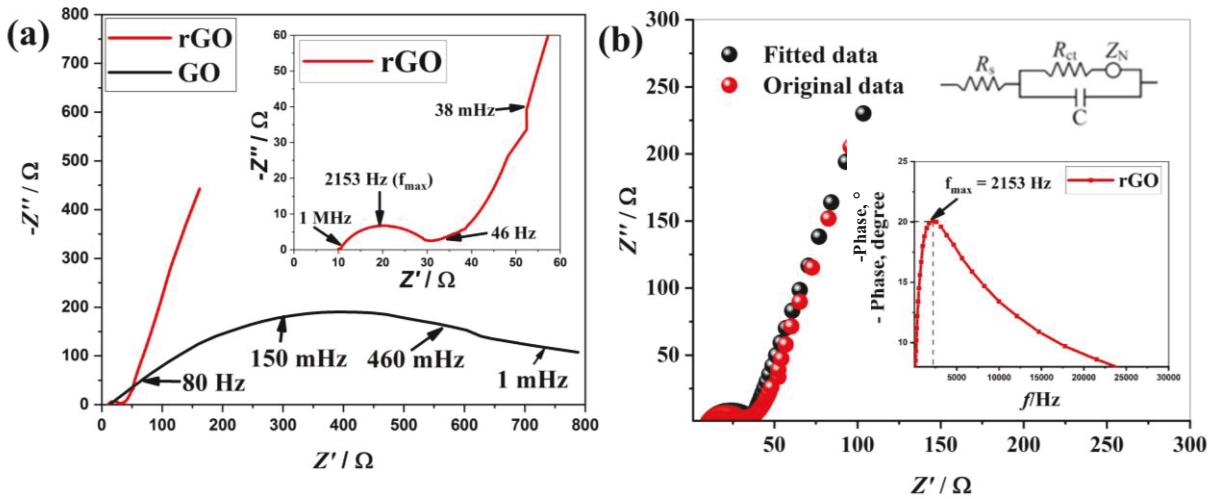

Figure 4. *(a) EIS measurements of GO and rGO symmetric cells (inset: enlarged Nyquist plot of rGO) (b) EIS Nyquist plot of rGO with fitted data (inset: electrical equivalent circuit model and Bode phase plot of the rGO)*

Tafel polarization test of symmetric cells

Tafel graph represents the variation of (log J) along with applied potential. The key element of the Tafel plot is the exchange current density (J_0). By measuring the intercept of a curve extrapolated linear section at zero overpotential, it is possible to determine a value of J_0 [39]. Figure 3(d) represents the Tafel polarization curve of GO and rGO symmetric cells. The Tafel curve of rGO has a

higher slope as compared to GO, which means the rGO has higher catalytic activity towards the I_3^- reduction due to the better conductivity, lower value of R_{ct} and large number of defects on rGO sheets, which enhanced the catalytic performance of rGO-CE.

Conclusions

In this report, an easy, cost-effective and environmentally friendly process was used to synthesize rGO by utilizing KOH and NaOH as the reducing agent. The KOH and NaOH reducing agent can facilitate the large number of defects in rGO, which enhances the electrocatalytic performance of CE. The morphological results illustrate that the synthesized rGO has exfoliated sheet morphology, whereas the Raman spectroscopy study reveals that the rGO exhibits low crystallite size with a large number of defects. The electrochemical characteristics indicate that the rGO-CE has a low value of R_{ct}, high cathodic current density and high Tafel slope, demonstrating the significant catalytic activity of rGO-CE towards the I_3^- reduction. The improved catalytic performance of rGO-CE can be attributed to better conductivity, high surface area and the presence of a large number of defects in the material, which not only increased the contact area of the electrode/electrolyte interface but also facilitated more catalytic sites for proper diffusion of redox electrolyte ions. It can be inferred from the results of the evaluation of the catalytic performance of rGO-CE in this study that the rGO is a potential choice as an efficient and metal-free CE for DSSCs with remarkable catalytic performance.

Conflict of interest: *The authors express no conflict of interest.*

Acknowledgment: *All authors are grateful to the MRC, MNITJ India, for facilitating different characterization techniques for this study.*

References

[1] R. Bajpai, S. Roy, N. Koratkar, D. S. Misra, NiO nanoparticles deposited on graphene platelets as a cost-effective counter electrode in a dye sensitized solar cell, *Carbon* **56** (2013) 56-63. https://doi.org/10.1016/j.carbon.2012.12.087

[2] M. K. Nazeeruddin, E. Baranoff, M. Grätzel, Dye-sensitized solar cells: A brief overview, *Solar Energy* **85** (2011) 1172-1178. https://doi.org/10.1016/j.solener.2011.01.018

[3] K. Rokesh, A. Pandikumar, K. Jothivenkatachalam, Dye sensitized solar cell: A summary, *Materials Science Forum* **771** (2014) 1-24. https://doi.org/10.4028/www.scientific.net/MSF.771.1

[4] T. N. Murakami, M. Grätzel, Counter electrodes for DSC: Application of functional materials as catalysts, *Inorganica Chimica Acta* **361** (2008) 572-580. https://doi.org/10.1016/j.ica.2007.09.025

[5] A. Dubey, S. Dave, M. Lakhani, A. Sharma, Applications of graphene for communication, electronics and medical fields, 2016 *International Conference on Electrical, Electronics, and Optimization Techniques, (ICEEOT)* (2016) 2435-2439. https://doi.org/10.1109/ICEEOT.2016.7755131

[6] A. P. A. Raju, Production and Applications of Graphene and Its Composites, *Doctoral Thesis*, *The University of Manchester* (2015). https://pure.manchester.ac.uk/ws/portalfiles/portal/61846537/FULL_TEXT.PDF

[7] V. Singh, D. Joung, L. Zhai, S. Das, S. I. Khondaker, S. Seal, Graphene based materials: Past, present and future, *Progress in Materials Sci*ence **56** (2011) 1178-1271. https://doi.org/10.1016/j.pmatsci.2011.03.003

[8] J. Li, X. Zeng, T. Ren, E. Van der Heide, The Preparation of Graphene Oxide and Its Derivatives and Their Application in Bio-Tribological Systems, *Lubricants* **2** (2014) 137-161. https://doi.org/10.3390/lubricants2030137
[9] S. Priyadarsini, S. Mohanty, S. Mukherjee, S. Basu, M. Mishra, Graphene and graphene oxide as nanomaterials for medicine and biology application, *Journal of Nanostructure in Chem*istry **8** (2018) 123-137. https://doi.org/10.1007/s40097-018-0265-6
[10] V. Sharma, Y. Jain, M. Kumari, R. Gupta, S. K. Sharma, K. Sachdev, Synthesis and Characterization of Graphene Oxide (GO) and Reduced Graphene Oxide (rGO) for Gas Sensing Application, *Macromolecular Symp*osia **376** (2017) 1700006. https://doi.org/10.1002/masy.201700006
[11] D. Li, M. B. Müller, S. Gilje, R. B. Kaner, G. G. Wallace, Processable aqueous dispersions of graphene nanosheets, *Nature Nanotechnology* **3** (2008) 101-105. https://doi.org/10.1038/nnano.2007.451
[12] A. Kommu, J. K. Singh, A review on graphene-based materials for removal of toxic pollutants from wastewater, *Soft Mater*ials **18** (2020) 297-322. https://doi.org/10.1080/1539445X.2020.1739710
[13] Y. Liu, C. Chen, L. Liu, G. Zhu, Q. Kong, R. Hao, W. Tan, Rheological behavior of high concentrated dispersions of graphite oxide, *Soft Materials* **13** (2015) 167-175. https://doi.org/10.1080/1539445X.2015.1055004
[14] H. Kumar, R. Sharma, A. Yadav, R. Kumari, Recent advancement made in the field of reduced graphene oxide-based nanocomposites used in the energy storage devices: A review, *Journal of Energy Storage* **33** (2021) 102032. https://doi.org/10.1016/j.est.2020.102032
[15] S. Stankovich, D. A. Dikin, R. D. Piner, K. A. Kohlhaas, A. Kleinhammes, Y. Jia, Y. Wu, S. T, Naguyen, R. S. Ruoff, Synthesis of graphene-based nanosheets via chemical reduction of exfoliated graphite oxide, *Carbon* **45** (2007) 1558-1565. https://doi.org/10.1016/j.carbon.2007.02.034
[16] M. S. Khan, R. Yadav, R. Vyas, A. Sharma, M. K. Banerjee, K. Sachdev, Synthesis and evaluation of reduced graphene oxide for supercapacitor application, *Materials Today: Proceedings* **30(1)** (2020) 153-156. https://doi.org/10.1016/j.matpr.2020.05.403
[17] G. Hou, J. Gao, J. Xie, B. Li, Preparation and properties characterization of gallic acid epoxy resin/succinic anhydride bionanocomposites modified by green reduced graphene oxide, *Soft Mater*ials **14** (2016) 27-37. https://doi.org/10.1080/1539445X.2015.1098704
[18] C. Gómez-Navarro, J. C. Meyer, R. S. Sundaram, A. Chuvilin, S. Kurasch, M. Burghard, K. Kern, U. Kaiser, Atomic Structure of Reduced Graphene Oxide, *Nano Letters* **10** (2010) 1144-1148. https://doi.org/10.1021/nl9031617
[19] S. Joshi, R. Siddiqui, P. Sharma, R. Kumar, G. Verma, A. Saini, Green synthesis of peptide functionalized reduced graphene oxide (rGO) nano bioconjugate with enhanced antibacterial activity, *Scientific Reports* **10** (2020) 9441. https://doi.org/10.1038/s41598-020-66230-3
[20] E. Vatandost, A. Ghorbani-HasanSaraei, F. Chekin, S. Naghizadeh Raeisi, S.A. Shahidi, Green tea extract assisted green synthesis of reduced graphene oxide: Application for highly sensitive electrochemical detection of sunset yellow in food products, *Food Chemistry: X* **6** (2020) 100085. https://doi.org/10.1016/j.fochx.2020.100085
[21] G. Calderón-Ayala, M. Cortez-Valadez, P. G. Mani-Gonzalez, R. B. Hurtado, J. I. Contreras-Rascón, R. C. Carrillo-Torres, M. E. Zayas, S. J. Castillo, A. R. Hernández-Martínez, M. Flores-Acosta, Green synthesis of reduced graphene oxide using ball milling, *Carbon Letters* **21** (2017) 93-97. https://doi.org/10.5714/CL.2017.21.093
[22] P. Chettri, V. S. Vendamani, A. Tripathi, A.P. Pathak, A. Tiwari, Self-assembly of functionalised graphene nanostructures by one step reduction of graphene oxide using aqueous extract of

Artemisia vulgaris, *Applied Surface Science* **362** (2016) 221-229. https://doi.org/10.1016/j.apsusc.2015.11.231

[23] L. Gan, B. Li, Y. Chen, B. Yu, Z. Chen, Green synthesis of reduced graphene oxide using bagasse and its application in dye removal: A waste-to-resource supply chain, *Chemosphere* **219** (2019) 148-154. https://doi.org/10.1016/j.chemosphere.2018.11.181

[24] D. Jhankal, M. Saquib, K. K. Jhankal, K. Sachdev, Charge storage kinetics of MoS_2 flower decorated reduced graphene oxide for quasi solid-state symmetric supercapacitor, *Journal of Physics and Chemistry of Solids* **173** (2023) 111117. https://doi.org/10.1016/j.jpcs.2022.111117

[25] P. Gu, D. Yang, X. Zhu, H. Sun, P. Wangyang, J. Li, H. Tian, Influence of electrolyte proportion on the performance of dye-sensitized solar cells, *AIP Advances* **7** (2017) 105219. https://doi.org/10.1063/1.5000564

[26] A. C. Ferrari, J. C. Meyer, V. Scardaci, C. Casiraghi, M. Lazzeri, F. Mauri, S. Piscanec, D. Jiang, K.S. Novoselov, S. Roth, A.K. Geim, Raman spectrum of graphene and graphene layers, *Physical Reviews Lett*ers **97** (2006) 187401. https://doi.org/10.1103/PhysRevLett.97.187401

[27] S. Sarker, K.-S. Lee, H. W. Seo, Y.-K. Jin, D. M. Kim, Reduced graphene oxide for Pt-free counter electrodes of dye-sensitized solar cells, *Solar Energy* **158** (2017) 42-48. https://doi.org/10.1016/j.solener.2017.09.029

[28] B. Zhu, H. Li, Y. Chen, H. Liu, Facile synthesis and high volumetric capacitance of holey graphene film for supercapacitor electrodes with optimizing preparation conditions, *Soft Materials* **20** (2022) 137-148. https://doi.org/10.1080/1539445X.2021.1928703

[29] A. Kaushal, S. K. Dhawan, V. Singh, Determination of crystallite size, number of graphene layers and defect density of graphene oxide (GO) and reduced graphene oxide (RGO), *AIP Conference Proceedings* **2115** (2019) 030106. https://doi.org/10.1063/1.5112945

[30] M. Sharma, S. Rani, D. K. Pathak, R. Bhatia, R. Kumar, I. Sameera, Temperature dependent Raman modes of reduced graphene oxide: Effect of anharmonicity, crystallite size and defects, *Carbon* **184** (2021) 437-444. https://doi.org/10.1016/j.carbon.2021.08.014

[31] N. P. D. Ngidi, M. A. Ollengo, V. O. Nyamori, Effect of doping temperatures and nitrogen precursors on the physicochemical, optical, and electrical conductivity properties of nitrogen-doped reduced graphene oxide, *Materials* **12** (2019) 3376. https://doi.org/10.3390/ma12203376

[32] Z. Wang, P. Li, Y. Chen, J. He, J. Liu, W. Zhang, Y. Li, Phosphorus-doped reduced graphene oxide as an electrocatalyst counter electrode in dye-sensitized solar cells, *Journal of Power Sources* **263** (2014) 246-251. https://doi.org/10.1016/j.jpowsour.2014.03.118

[33] F. Yu, Y. Shi, W. Yao, S. Han, J. Ma, A new breakthrough for graphene/carbon nanotubes as counter electrodes of dye-sensitized solar cells with up to a 10.69 % power conversion efficiency, *Journal of Power Sources* **412** (2019) 366-373. https://doi.org/10.1016/j.jpowsour.2018.11.066

[34] G. Yue, J.-Y. Lin, S.-Y. Tai, Y. Xiao, J. Wu, A catalytic composite film of MoS_2/graphene flake as a counter electrode for Pt-free dye-sensitized solar cells, *Electrochimca Acta* **85** (2012) 162-168. https://doi.org/10.1016/j.electacta.2012.08.040

[35] A. Sarkar, A. K. Chakraborty, S. Bera, NiS/rGO nanohybrid: An excellent counter electrode for dye sensitized solar cell, *Solar Energy Materials and Solar Cells* **182** (2018) 314-320. https://doi.org/10.1016/j.solmat.2018.03.026

[36] J. Zhao, J. Ma, X. Nan, B. Tang, Application of non-covalent functionalized carbon nanotubes for the counter electrode of dye-sensitized solar cells, *Organic Electronics* **30** (2016) 52-59. https://doi.org/10.1016/j.orgel.2015.11.032

[37] Q. Wang, J. E. Moser, M. Grätzel, Electrochemical impedance spectroscopic analysis of dye-sensitized solar cells, *The Journal of Physical Chemistry B* **109** (2005) 14945-14953. https://doi.org/10.1021/jp052768h

[38] T. Shen, J. Tian, L. Lv, C. Fei, Y. Wang, T. Pullerits, G. Cao, Investigation of the role of Mn dopant in CdS quantum dot sensitized solar cell, *Electrochimica Acta* **191** (2016) 62-69. https://doi.org/10.1016/j.electacta.2016.01.056

[39] U. Mehmood, N. A. Karim, H. F. Zahid, T. Asif, M. Younas, Polyaniline/graphene nanocomposites as counter electrode materials for platinum free dye-sensitized solar cells (DSSCSs), *Materials Letters* **256** (2019) 126651. https://doi.org/10.1016/j.matlet.2019.126651